ChemPubSoc Europe

DOI: 10.1002/cplu.201700551

CHEMPLUSCHEM Full Papers

Ferrocenyl GNA Nucleosides: A Bridge between Organic and Organometallic Xeno-nucleic Acids**

Joanna Skiba,[a] Qing Yuan,[b] Alexander Hildebrandt,[b] Heinrich Lang,[b] Damian Trzybiński,[c] Krzysztof Woźniak,[c] Ria K. Balogh,[d] Béla Gyurcsik,[d] Valerije Vrček,[e] and Konrad Kowalski*[a]

The enantioselective synthesis and electrochemistry of the first ferrocenyl GNA nucleosides is reported. These compounds were obtained by a Sharpless asymmetric dihydroxylation reaction of [3-(*N*1-thyminyl)-1-(ferrocenyl)]propene as *S*,*R* and *R*,*S* enantiomers in about 70% yield with enantiomeric excesses of >99% and 71%, respectively. The absolute configurations of the chiral carbon atoms in the nucleosides were assigned by single-crystal X-ray diffraction analysis of the methyl derivatives in the solid state. The compounds were also studied with circular dichroism (CD) spectroscopy in solution. The enantiomeric relationship between the *S*,*R* and *R*,*S* isomers was confirmed by the near-mirror-image CD spectra. The redox properties of the nucleosides and their methylated derivatives were investigated using cyclic voltammetry. The cyclic voltammograms revealed reversible redox processes for the entire series of compounds at potentials of −25 mV (for nonmethylated derivatives) and 75 mV (for methylated derivatives) versus the ferrocene/ferrocenium reference redox couple.

Introduction

The basic chemical structure of nucleic acids (e.g., deoxyribonucleic acid, DNA, and ribonucleic acid, RNA) is common and independent of the taxonomic rank, for all living and extinct species in the biosphere. Nucleic acids consist of canonical nucleosides interlinked with phosphodiester bonds to form higher-order helical and other topology structures.[1,2] Nucleoside units are built of five canonical nucleobases (adenine, guanine, thymine cytosine and uracil) which are attached to the anomeric C atoms of D-deoxyribofuranose (in DNA) and D-ribofuranose (in RNA) sugars, respectively. Furthermore, the nucleosides can contain noncanonical (epigenetic) modified nucleobases. Although the biological function of such modified nucleobases is still far from being fully understood, it is apparent that they play crucial roles, for example, in gene expression and in gene silencing.[3] In contrast, modified nucleosides and their components have been in the focus of chemical studies for decades.[4] As a result, many modified nucleosides have found therapeutic applications, mainly as antiviral and anticancer drugs.[5,6]

Xeno-nucleic acid (XNA) chemistry is aimed at developing and investigating entirely new classes of artificial nucleic acids that have the ability to carry genetic information, undergo molecular evolution, and serve as tools for molecular biology studies.[7–9] XNA chemistry also sheds light on prebiotic chemistry and the origin of life on planet Earth. Formally, the term XNA denotes a nucleic acid that does not exist in the living world and whose D-(deoxy)ribofuranose backbone is replaced by an alternative sugar or nonsugar moiety.[7] According to the above definition, progress in XNA chemistry relies on the development of new artificial nucleoside building blocks.

Until recently, there have been two separate families of XNA nucleosides described in the literature. The first major group consists of purely organic molecules, whereas the second, of fewer examples, consists of organometallic ferrocenyl compounds. A simplified "phylogenetic-like tree" showing both classes of nucleosides is presented in Figure 1.

The arrows in Figure 1 tentatively represent gradual structural changes on going from the glycol nucleic acid (GNA) nucleoside,[10–13] followed by flexible nucleic acid (FNA) nucleosides[14,15] through canonical thymidine nucleosides and finally to their more structurally distant congeners such as arabino nucleic acid (ANA),[16] 2′-fluoro-arabino nucleic acid (FANA),[17] and α-L-threofuranose nucleic acid (TNA)[18] nucleosides. Branches consist of aminopropyl nucleic acid (APNA) nucleo-

[a] *Dr. J. Skiba, Dr. K. Kowalski*
Faculty of Chemistry
Department of Organic Chemistry
University of Łódź, Tamka 12, 91-403 Łódź (Poland)
E-mail: kondor15@wp.pl

[b] *Q. Yuan, Dr. A. Hildebrandt, Prof. Dr. H. Lang*
Faculty of Natural Sciences
Institute of Chemistry, Inorganic Chemistry
Technische Universität Chemnitz, 09107 Chemnitz (Germany)

[c] *Dr. D. Trzybiński, Prof. Dr. K. Woźniak*
Biological and Chemical Research Centre
Department of Chemistry
University of Warsaw, Żwirki i Wigury 101, 02-089 Warszawa (Poland)

[d] *R. K. Balogh, Prof. Dr. B. Gyurcsik*
Faculty of Chemistry
Department of Inorganic and Analytical Chemistry
University of Szeged, Dom ter 7., 6720 Szeged (Hungary)

[e] *Prof. Dr. V. Vrček*
Faculty of Pharmacy and Biochemistry
University of Zagreb
Ante Kovačića 1, 10000 Zagreb (Croatia)

[**] *GNA = glycol nucleic acid*

Supporting information and the ORCID identification number(s) for the author(s) of this article can be found under https://doi.org/10.1002/cplu.201700551.

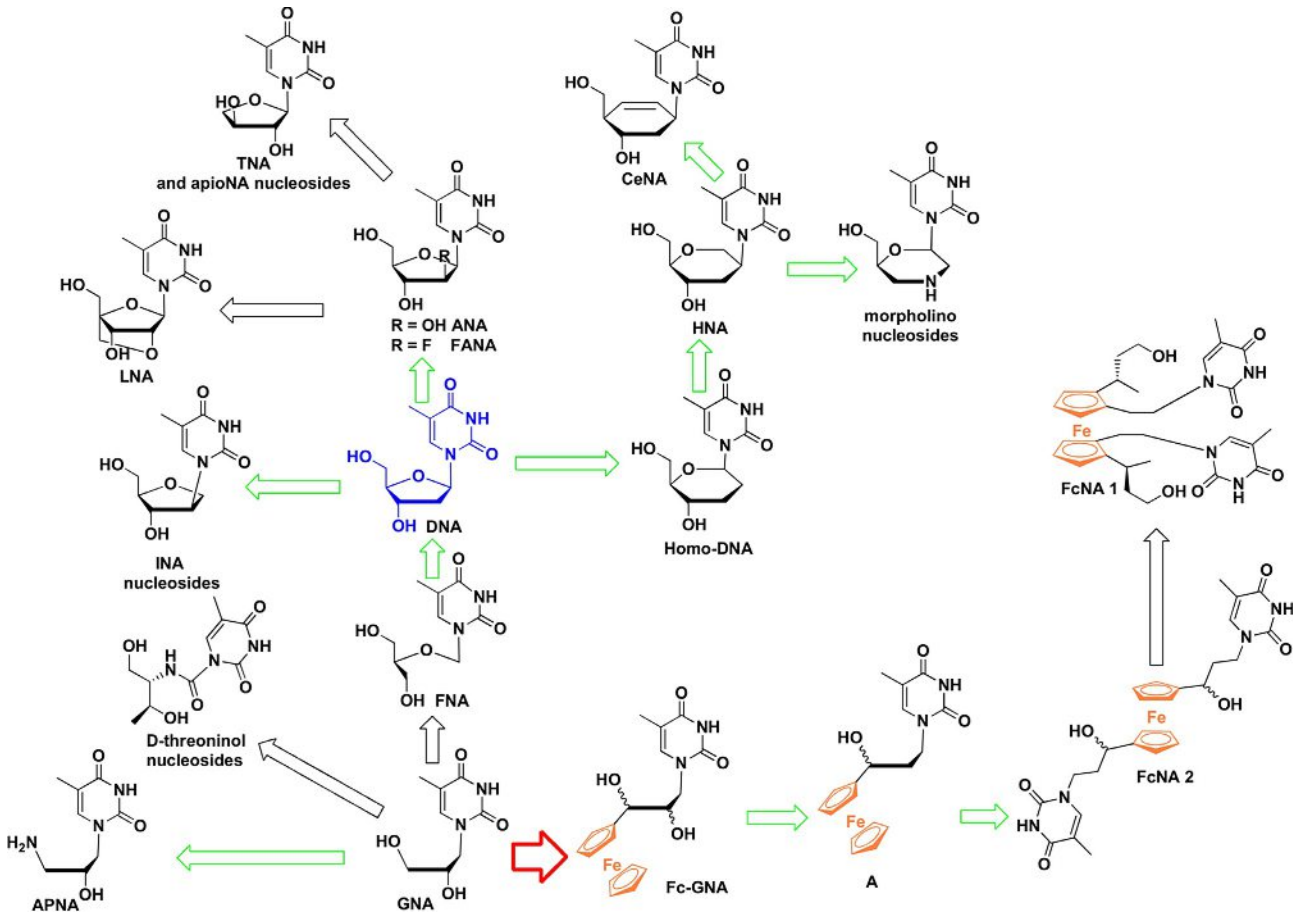

Figure 1. Simplified phylogenetic-like tree for XNA nucleosides shown with thymine as an exemplary nucleobase. The transition from organic to ferrocenyl nucleosides is marked by red arrows. Green arrows denote relatively close structural relationships between nucleosides, and black arrows pertain to more distant structural similarities.

sides,[19] D-threoninol nucleosides,[20] isonucleosides (INA)[21] and locked nucleic acid (LNA) nucleosides.[22] Branched from DNA are the homo-DNA,[23] hexitol nucleic acid (HNA),[24] cyclohexene nucleic acid (CeNA)[25] and morpholino nucleic acid nucleosides.[26] Remarkably different from all the above purely organic nucleosides are compounds containing the ferrocenyl moiety. Members of this family are organized into a separate branch on the phylogenetic-like tree in Figure 1. Ferrocene itself is a redox-active, aromatic organometallic molecule with a characteristic 3D sandwich-type structure. Ferrocenyl derivatives have found a plethora of applications in catalysis,[27] material sciences,[28] as well as in biology and medicinal chemistry.[29–31]

The rationale for the introduction of the ferrocenyl group into the nucleoside skeleton is well justified by the expectation of obtaining new classes of genetic information carriers having additional redox-active properties. Furthermore, it has been reported that some planar chiral ferrocenyl nucleosides show cytotoxic activity against human cancer cells with IC_{50} values in the low micromolar concentration range.[32,33] There are two general strategies toward the synthesis of ferrocenyl nucleic acids. The first relies on chemical or enzymatic oligomerization/incorporation of ferrocenyl nucleosides into the biopolymer and the second uses postsynthetic incorporation of ferrocenyl moieties into oligonucleotide strands. These strategies have been discussed in an excellent review.[34] The development of ferrocenyl XNA nucleosides and nucleic acids is a hot topic in chemistry.

The first ferrocenyl nucleoside FcNA1 (Figure 1) was reported in 2012 by Tucker and co-workers.[35] Following the challenging multi-step synthesis, FcNA1 was successfully polymerized on a nucleic acid synthesizer to afford the first ever ferrocenyl nucleic acid oligomers.[35] The oligomer was soluble in aqueous phosphate buffer at physiological pH, similar to natural nucleic acids. Cyclic voltammetry (CV) was used to study the redox processes of the FcNA1 oligomer.[35] The resulting cyclic voltammogram showed a quasi-reversible wave centered at 212 mV versus a Ag/AgCl reference, which originates from the oxidation–reduction of the ferrocenyl backbone moiety.

Recently, our group reported on the synthesis of the ferrocenyl nucleoside FcNA2 (Figure 1), which is the second known representative of ferrocenyl nucleosides.[36] Compound FcNA2 shares important common structural features with FcNA1, pertaining to the replacement of the D-ribofuranose backbone of canonical nucleoside by the 1,1′-disubstituted ferrocenyl moiety. Such a replacement forces the ferrocenyl group to be in the backbone of the nucleic acid strand. Until now, FcNA1 and FcNA2 remain unrelated to the rest of the XNA nucleoside family shown in Figure 1.

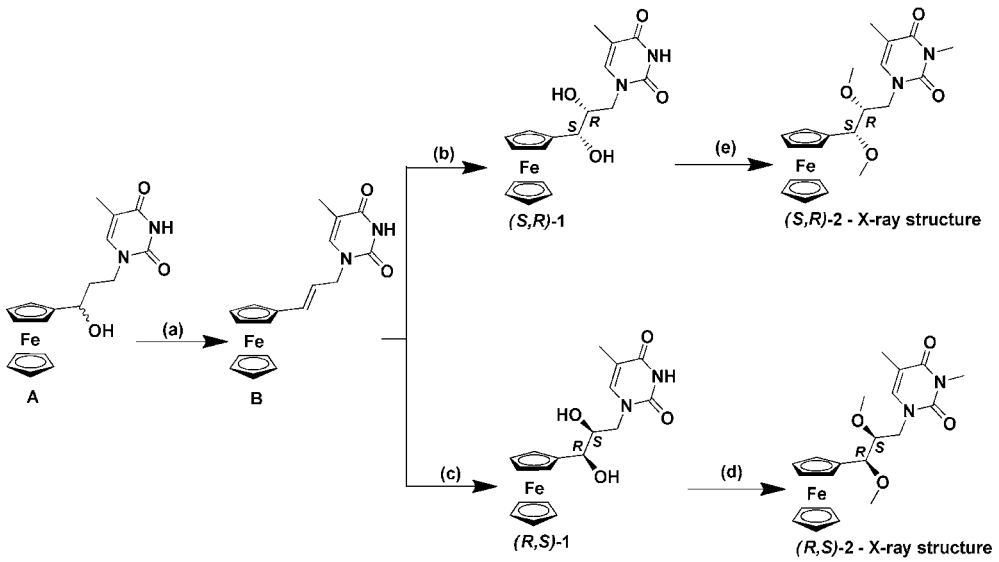

Scheme 1. Synthesis of nucleosides (*S*,*R*)-**1** and (*R*,*S*)-**1** and their methylated derivatives (*S*,*R*)-**2** and (*R*,*S*)-**2**. Reagents and conditions: a) $Yb(CF_3SO_3)_3$, ethylene glycol, 110 °C, 30 min; b) hydroquinidine-2,5-diphenyl-4,6-pyrimidinediyl diether [$(DHQD)_2Pyr$], $K_2OsO_2(OH)_4$, $K_3Fe(CN)_6$, K_2CO_3, water/acetonitrile (1:1 v/v), ambient temperature, 3 h; c) hydroquinine 2,5-diphenyl-4,6-pyrimidinediyl diether [$(DHQ)_2Pyr$], $K_2OsO_2(OH)_4$, $K_3Fe(CN)_6$, K_2CO_3, water/acetonitrile (1:1 v/v), ambient temperature, 3 h; d) and e) NaH, DMF, ambient temperature, 2 h, then CH_3I, ambient temperature, 20 h.

Herein, we report on the enantioselective synthesis, electrochemistry and DFT calculations of the ferrocenyl glycol nucleic acid (Fc–GNA) nucleosides (*S*,*R*)-**1** and (*R*,*S*)-**1** and their methylated derivatives (*S*,*R*)-**2** and (*R*,*S*)-**2** (Scheme 1). Furthermore, methylated derivatives were studied with X-ray diffraction and circular dichroism (CD) spectroscopy. The discussed nucleosides are close relatives to quasi-nucleoside **A** (Figure 1),[37] nucleoside FcNA2[36] and, most importantly, to metal-free GNA nucleosides.[10–13] Therefore, compounds (*S*,*R*)-**1** and (*R*,*S*)-**1** could be considered as "missing links", bridging the purely organic XNA nucleosides with organometallic ones.

Results and Discussion

Synthesis

GNA nucleosides are characterized by a single stereogenic carbon atom center in their molecular structure.[10–13] In contrast to that, the Fc–GNA derivatives studied herein possess two vicinal stereogenic carbon atom centers. Therefore, the synthesis of the enantiomerically pure Fc–GNA nucleosides requires either a separation of racemic mixtures or the synthesis of pure enantiomers. In the course of our work, we decided to utilize the latter approach. The synthetic methodology for the nucleosides (*S*,*R*)-**1** and (*R*,*S*)-**1**, their methylated derivatives (*S*,*R*)-**2** and (*R*,*S*)-**2** is summarized in Scheme 1.

The synthesis starts with alcohol **A**, which was prepared according to a previous report.[37] In the next step, dehydration of compound **A** was achieved by its treatment with ytterbium(III) trifluoromethanesulfonate in ethylene glycol at 110 °C. This reaction afforded [3-(*N*1-thyminyl)-1-(ferrocenyl)]propene (**B**)[37] in 66% yield. Notably, the reported literature method for the synthesis of **B** was less effective and gave **B** in only 32% yield.[37] Alkene **B** was then utilized as a substrate for the preparation of the chiral α,β-dihydroxy (*S*,*R*)-**1** and (*R*,*S*)-**1** isomers. To achieve this goal, a Sharpless catalytic asymmetric dihydroxylation was applied.[38] As a starting point in the search for the most suitable reaction conditions, we used the results of asymmetric dihydroxylation reactions conducted on relatively simple substrates such as vinylferrocene and homoallylferrocene.[39] Based on these initial data, we were able to develop suitable reaction conditions for the asymmetric hydroxylation of substrate **B**. Accordingly, treatment of **B** with 3 equivalents of $K_3Fe(CN)_6$ and K_2CO_3, 4 mol% $K_2OsO_2(OH)_4$ and 10 mol% hydroquinidine-2,5-diphenyl-4,6-pyrimidinediyl diether [$(DHQD)_2Pyr$] in a water/acetonitrile solvent mixture at ambient temperature for 3 h afforded nucleoside (*S*,*R*)-**1** in 72% yield and >99% *ee*. Using the same reaction conditions, but with hydroquinine 2,5-diphenyl-4,6-pyrimidinediyl diether [$(DHQ)_2Pyr$] as a ligand, allowed the isolation of a (*R*,*S*)-**1** isomer in 70% yield and in 71 *ee*. Nucleosides (*S*,*R*)-**1** and (*R*,*S*)-**1** are air-stable, yellow crystalline solids. They were characterized by spectroscopic methods, including ^1H NMR, ^{13}C NMR and IR spectroscopy, mass spectrometry, and elemental analysis. To assign the absolute configurations at the stereogenic centers in both products, we attempted to obtain X-ray-quality single crystals. However, these attempts failed. Therefore, the nucleosides were transformed into their methylated derivatives according to a literature method.[36] This procedure comprises the reaction of either nucleoside with NaH and MeI (Scheme 1) which does not influence stereochemical configuration. As a consequence, the absolute configuration at the stereogenic centers was retained. The respective methylation reaction afforded compounds (*S*,*R*)-**2** and (*R*,*S*)-**2** as yellow crystalline solids in approximately 30% yield. These compounds were characterized by spectroscopic methods, mass spectrometry, and elemental analysis as well as by single-crystal X-ray diffraction analysis.

X-ray diffraction study of enantiomers (*S*,*R*)-2 and (*R*,*S*)-2

The molecular structure of the nucleosides (*S*,*R*)-**2** and (*R*,*S*)-**2** in the solid state was determined by single-crystal X-ray diffraction analysis. Crystals suitable for these measurements were grown from saturated DMSO solutions at ambient temperature over 3 days. The molecular diagrams showing atom numbering for (*S*,*R*)-**2** and (*R*,*S*)-**2** are shown in Figure 2. The crystallographic details are summarized in Table S1 in the Supporting Information. The bond lengths and valence angles are summarized in Tables S2–S7.

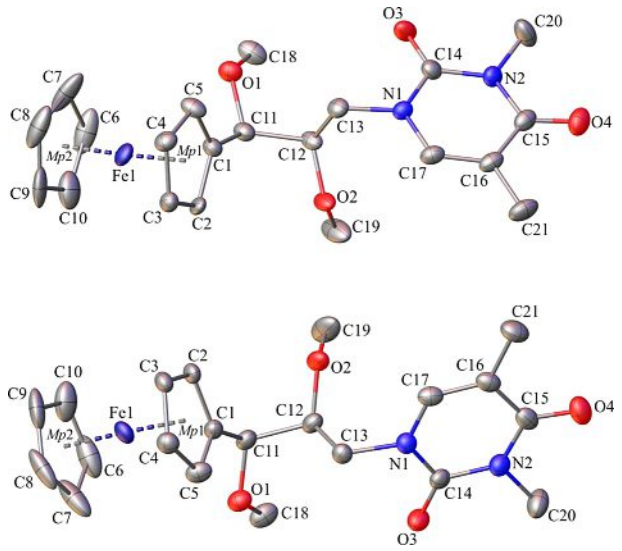

Figure 2. The molecular diagram of (*S*,*R*)-**2** (top) and (*R*,*S*)-**2** (bottom) at the 50% probability level. Mp1 and Mp2 correspond to midpoints of the substituted and unsubstituted cyclopentadienyl ligands, respectively. Hydrogen atoms have been omitted for clarity. Selected bond lengths [Å] and angles [°]: (*S*,*R*)-**2**/(*R*,*S*)-**2**: Fe1–Mp1, 1.638(2)/1.639(2); Fe1–Mp2, 1.644(3)/1.643(2); C1–C11, 1.497(6)/1.497(1); C11–C12, 1.541(6)/1.544(4); N1–C13, 1.464(6)/1.470(4); O1–C11, 1.431(6)/1.428(4); O2–C12, 1.422(6)/1.423(4); O1–C18, 1.429(6)/1.424(4); O2–C19, 1.421(6)/1.422(4); N1–C17, 1.368(6)/1.374(4); C1–C11–C12–C13, −53.6(5)/53.6(3); N1–C13–C2–C11, −171.9(4)/171.6(3).

The methylated nucleosides (*S*,*R*)-**2** and (*R*,*S*)-**2** crystallize in the chiral orthorhombic $P2_12_12_1$ space group with one enantiomer of the respective compound in the asymmetric part of the unit cell. The absolute configurations at the stereogenic centers C11 and C12 (Figure 2) were unambiguously assigned as (*S*,*R*)-**2** and (*R*,*S*)-**2**, respectively. The same absolute configuration can be assigned for nonmethylated (*S*,*R*)-**1** and (*R*,*S*)-**1** nucleosides. Alignment of molecules of (*S*,*R*)-**2** and (*R*,*S*)-**2** (after digital inversion with the Mercury software) reveals that they are almost isostructural with the root-mean-square deviation (RMSD) of the atomic positions value equal to 0.0162 Å. A superimposed representation (after computed inversion) of the enantiomers (*S*,*R*)-**2** and (*R*,*S*)-**2** is shown in Figure 3.

As well as the assignment of the absolute stereochemistry, single-crystal X-ray diffraction analysis unambiguously confirmed that the thymine moiety is bonded to the carbon linker through the N1 atom. The ferrocenyl moiety adopts an eclipsed conformation with the average C1–Mp1–Mp2–C6

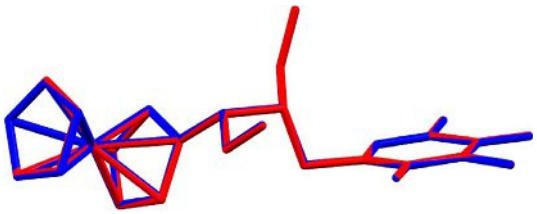

Figure 3. An overlay of the enantiomers from the crystal structures of (*S*,*R*)-**2** (blue) and (*R*,*S*)-**2** (red); RMSD = 0.0162 Å; the molecule of (*R*,*S*)-**2** is inverted.

(Mp = midpoint of the cyclopentadienyl ligand) angles of −1.13° and 0.81° for (*S*,*R*)-**2** and (*R*,*S*)-**2**, respectively. The geometry of the methylated thymine does not show significant differences compared with the literature.[34] In both structures the methylated thymine moiety points away from the ferrocenyl group. The dihedral angles between the plane of the thymine and substituted cyclopentadienyl ring in (*S*,*R*)-**2** and (*R*,*S*)-**2** are 113.99(19)° and 114.10(12)°, respectively. In the investigated compounds, adjacent molecules are involved in weak C–H···O hydrogen bonds, which results in the formation of the complex supramolecular framework (Figure S9 and Tables S8 and S9).

UV/Vis absorption and CD spectroscopy and DFT calculations

The methylated nucleosides (*S*,*R*)-**2** and (*R*,*S*)-**2** were subjected to UV/Vis absorption measurements in dichloromethane solution (Figure 4). The pattern of the absorption spectra is the same for both compounds within the limit of error of the measurement. The spectra show intense UV absorption bands below 300 nm, a less intense near-UV band at 330 nm and relatively weak absorptions in the visible region with the maximum at 438 nm (Table 1). Such a pattern of the absorption spectra corroborates with the literature spectroscopic data for ferrocene derivatives.[28d,40–45]

In order to get a more detailed insight into the nature of the experimentally observed electronic transitions, calculations

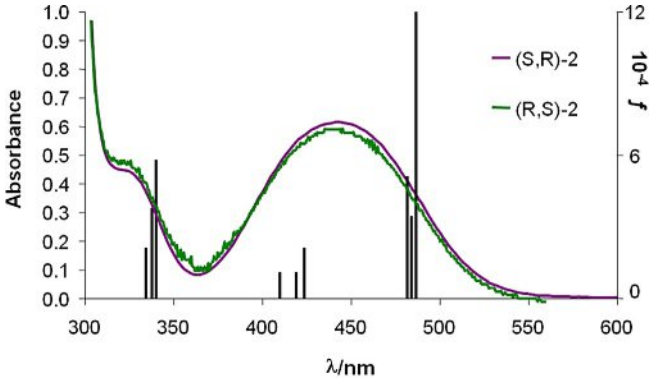

Figure 4. UV/Vis absorption spectra of (*S*,*R*)-**2** and (*R*,*S*)-**2** in dichloromethane solution normalized to 5.0×10^{-3} mol L^{-1} at ambient temperature and the TD-DFT-calculated electronic transitions for (*R*,*S*)-**2** (vertical bars; oscillator strengths are given on the right *y* axis).

Table 1. UV/Vis absorption data of compounds (*S*,*R*)-**2** and (*R*,*S*)-**2**.

Compound	ε [L mol^{-1} cm^{-1}]	λ_{max} [nm]
(*S*,*R*)-**2**	123	438
	88	330 (sh)
(*R*,*S*)-**2**	118	438
	87	330 (sh)

were performed for (*R*,*S*)-**2**. The B3LYP/6-31G(d)/SDD level of theory was used for geometry optimization, and the BPW91/6-311G(d)/SDD level of theory was applied for time-dependent density functional theory (TD-DFT) calculations. The optimized geometry of (*R*,*S*)-**2** is shown in Figure S10, the frontier molecular orbitals are depicted in Figure 5, and calculation details are summarized in Tables S10 and S11.

As expected for the low-spin ferrocene derivative, the three highest lying occupied molecular orbitals HOMO, HOMO-1 and HOMO-2 in (*R*,*S*)-**2** dominantly correspond to the iron-centered $d_{x^2-y^2}$, d_{xy} and d_{z^2} atomic orbitals.[40–45] The lowest unoccupied molecular orbital (LUMO) of (*R*,*S*)-**2** has π-character and is delocalized over the thymine moiety. The two higher lying LUMO+1 and LUMO+2 molecular orbitals consist of iron-centered 3D-orbitals with contribution of the cyclopentadienyl π orbitals. The TD-DFT-calculated electronic absorption spectrum of (*R*,*S*)-**2** is shown in Figure 4. Only energies above 330 nm are considered as they refer to the experimentally measured CD spectrum in dichloromethane solution (Figure 6). The three calculated lowest energy transitions at 478.65, 478.29, and 472.89 nm agree with the position of the low-energy band observed in the UV/Vis spectrum of (*R*,*S*)-**2** at 438 nm. The first calculated low-energy band at 478.65 nm predominantly consists of HOMO to LUMO excitation, and can be assigned to a metal-to-ligand charge-transfer electronic transition. The two calculated bands centered at 478.29 and 472.89 nm include additional transitions with d–d character, for example, HOMO-1 to LUMO+1 and HOMO to LUMO+2 orbitals. The three calculated bands at 423.06, 420.50, and 425.57 nm have a low oscillator strength ($f \leq 0.0002$). They can be assigned as iron-centered transitions with some contribution of a HOMO-2 to LUMO transition. Finally, the calculated three highest energy transitions at 343.24, 342.75, and 338.55 nm correspond to the experimentally observed higher energy band at 330 nm. These transitions involve the HOMO to LUMO+1, HOMO-2 to LUMO+1 and HOMO-2 to LUMO+2 electronic transitions. Overall, calculated vertical excitation energies are consistent with the experimentally observed UV/Vis spectrum of (*R*,*S*)-**2** and provide a detailed insight into the nature of all relevant bands.

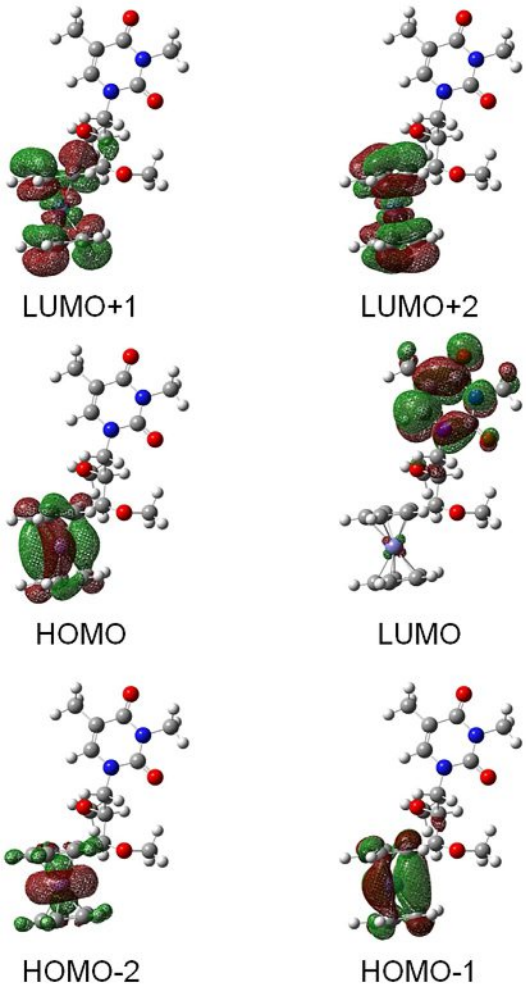

Figure 5. Contour plots of selected Kohn–Sham frontier molecular orbitals involved in calculated electronic transitions of (*R*,*S*)-**2**.

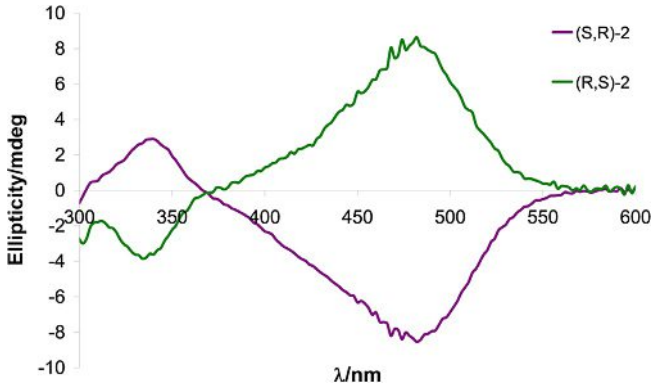

Figure 6. Baseline-corrected CD spectra of (*S*,*R*)-**2** and (*R*,*S*)-**2** in dichloromethane normalized to 5.0×10^{-3} mol L^{-1} at ambient temperature.

As described above, the absolute configurations of the enantiomers of **2** in the solid state were established by X-ray crystallography. With the following experiments, we aimed to correlate the established stereochemistry of both enantiomers with CD spectra in solution. CD spectra are excellent for establishing and predicting the absolute configurations for ferrocene derivatives.[46–48] Therefore, they can be used as guides for the assignment of the absolute configuration of new ferrocenyl nucleobases if X-ray crystal structures are not available. The CD spectra of both enantiomers (*S*,*R*)-**2** and (*R*,*S*)-**2** are shown in Figure 6. The (*S*,*R*)-**2** enantiomer shows a weak positive Cotton

effect in the d–d transition region between 310–370 nm and an intense negative signal between 370–550 nm with a minimum at approximately 480 nm. Conversely, an intense positive signal is observed for the (*R*,*S*)-**2** enantiomer between 370–550 nm with a weak negative signal at 310–370 nm.

The CD spectra of the (*S*,*R*)-**2** and (*R*,*S*)-**2** compounds are almost mirror images and can be used to determine the configurations of similar compounds and derivatives.

Electrochemistry

Ferrocenyl XNA nucleotides have been utilized as building blocks for construction of short redox-active nucleic acid strands[35] and ferrocenyl guanine conjugates have been used as standards for the quantification and analysis of DNA strands.[49] Furthermore, it has been shown that specifically designed, chelating oligonucleotides can self-assemble into metal-mediated nanowire structures.[50] Keeping in mind the predicted applications of ferrocenyl XNA nucleotides in biology and material sciences, the electrochemical properties of (*S*,*R*)-**1**, (*R*,*S*)-**1**, (*S*,*R*)-**2** and (*R*,*S*)-**2** were determined by cyclic voltammetry (CV) in dimethyl sulfoxide solutions containing weakly coordinating $[Bu_4N][B(C_6F_5)_4]$ (0.1 mol L^{-1}) as a supporting electrolyte at room temperature. The CV measurements were recorded at scan rates varying between 50 and 200 mV s^{-1}. All redox potentials were referenced against the FcH/FcH^+ redox couple ($E^{\circ\prime} = 0.00$ V) as recommended by IUPAC [$FcH = Fe(\eta^5\text{-}C_5H_5)_2$].[51] Table 2 shows the electrochemical data for the series of compounds studied. Figures 7 and 8 show the voltammograms of (*S*,*R*)-**1** and (*S*,*R*)-**2**, whereas Figures S11 and S12 show the voltammograms of (*R*,*S*)-**1** and (*R*,*S*)-**2**.

All compounds undergo a single Nernstian one-electron ferrocenyl-centered redox process, which under the experimental conditions applied occurs at $E^{\circ\prime} = -25$ mV [(*S*,*R*)-**1**, (*R*,*S*)-**1**] or 75 mV [(*S*,*R*)-**2**), ((*R*,*S*)-**2**] against the standard redox couple FcH/FcH^+. Compared to the nucleosides **1**, the potential for the ferrocenyl oxidation process of methyl derivatives **2** is counterintuitively shifted anodically by 100 mV. It is notable that the same anodic shift was reported for the FcNA2 nucleoside and its methylated derivative.[36] In order to explain these unexpected results, DFT calculations were performed for (*R*,*S*)-**1** and (*R*,*S*)-**2** derivatives at the SMD-B3LYP/6-31G(d)//B3LYP/6-31G(d)/SDD level of theory in dimethyl sulfoxide. The experimental redox potentials of (*R*,*S*)-**1** and its methylated analogue (*R*,*S*)-**2** were reproduced correctly by DFT calculations (Table 2 and Table S12). This might be surprising because the methoxy group in (*R*,*S*)-**2** is a stronger electron donor (has a positive induction effect) than the hydroxy group in (*R*,*S*)-**1**. However, in (*R*,*S*)-**1** the α-hydroxy group is involved in the formation of a strong intramolecular hydrogen bond to the neighboring β-hydroxy group (Figure S13). In the case of (*R*,*S*)-**2** no such intramolecular interaction exists. It is likely that owing to the intramolecular hydrogen bond formation in (*R*,*S*)-**1**, the proton-donating group (the α-OH group) increases its electron-donor ability toward the ferrocenyl group, making it more readily oxidized. This hypothesis was tested on ferrocenylmethanol (**I** in Figure S14) and its methylated derivative (**II** in Figure S14).

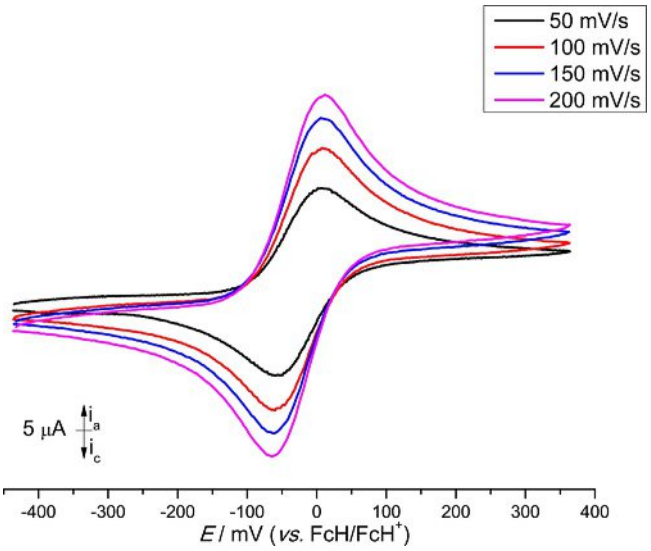

Figure 7. Cyclic voltammograms of dimethyl sulfoxide solutions containing (*S*,*R*)-**1** (1.0 mmol L^{-1}) at 25 °C; supporting electrolyte: $[N(nBu)_4][B(C_6F_5)_4]$ (0.1 mol L^{-1}).

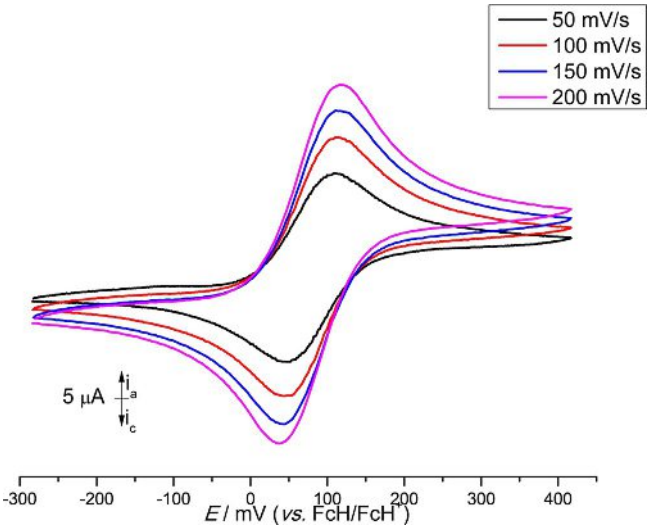

Figure 8. Cyclic voltammograms of dimethyl sulfoxide solutions containing (*S*,*R*)-**2** (1.0 mmol L^{-1}) at 25 °C; supporting electrolyte: $[N(nBu)_4][B(C_6F_5)_4]$ (0.1 mol L^{-1}).

Table 2. Voltammetric data for compounds (*S*,*R*)-**1**, (*R*,*S*)-**1**, (*S*,*R*)-**2**, and (*R*,*S*)-**2**.

Compound	Scan rate [mV s^{-1}]	$E^{\circ\prime}$[a] (ΔE_p)[b] [mV]	I_{pa}/I_{pc}[c]	Calcd $E^{\circ\prime}$[d] [mV]
(*S*,*R*)-**1**	50	−25 (68)	1.03	–
(*R*,*S*)-**1**	50	−25 (68)	1.08	−21.3
(*S*,*R*)-**2**	50	75(77)	1.08	–
(*R*,*S*)-**2**	50	75(65)	1.05	84.1

[a] $E^{\circ\prime}$ = formal potential. [b] ΔE_p = potential difference between oxidation and reduction. [c] I_{pa}/I_{pc} = ratio between anodic and cathodic peak currents. [d] Formal potential calculated at the SMD-B3LYP/6-31G(d)//B3LYP/6-31G(d)/SDD level of theory in DMSO as a model solvent.

These structures cannot take part in intramolecular hydrogen bonding, and therefore the calculated redox potentials are governed mainly by the inductive effects of the OH and OCH_3 groups. As expected, the calculated redox potential of **I** is shifted anodically by >10 mV compared to its methylated counterpart **II** (Table S12). This is consistent with the electron-withdrawing effect of the hydroxy group (negative induction effect), which renders the Fe center more electron deficient, and thus more difficult to oxidize. Therefore, we suggest that the strong intramolecular hydrogen bonding in (*R*,*S*)-**1** might at least in part be responsible for the experimentally observed redox potential. In summary, CV measurements confirmed that the ferrocenyl nucleosides studied have desirable electrochemical properties with respect to possible applications as redox-active bioprobes or conducting nanowires.

Conclusions

A Sharpless asymmetric dihydroxylation reaction was applied to obtain ferrocenyl GNA nucleosides. These are the first known representatives of redox-active organometallic GNAs to be reported and contribute to the expansion of the XNA family. Furthermore, our synthetic design overcomes the problem of a challenging multistep synthesis, as was the case for the planar chiral FcNA1 nucleoside. Both synthetic approaches, ours and that reported for FcNA1 are complementary in the sense that the former provides ferrocenyl GNA nucleosides with defined central chirality and the latter enables planar chiral molecules to be obtained.

The *S*,*R* and *R*,*S* absolute configuration of the chiral carbon atoms in the Fc–GNA nucleosides was assigned by X-ray crystallography of the methylated derivatives. Furthermore, CD spectroscopy of both isomers was conducted. The CD spectra are near-mirror images, reflecting the enantiomeric relationship between the compounds. Electrochemical studies revealed that each of the Fc–GNA nucleosides undergo reversible one-electron oxidations at potentials of -25 mV (for nonmethylated derivatives) and 75 mV (for methylated derivatives). Further synthetic, electrochemical and biological studies are needed to probe the usefulness of the herein reported Fc–GNA nucleosides as building blocks for oligonucleotide synthesis, as well as to examine their electrochemistry and biological activity.

Experimental Section

General information

All preparations were performed using standard Schlenk techniques. Chromatographic separations were performed using silica gel 60 (Merck, 230–400 mesh ASTM) or aluminum oxide (EcoChrom MP Biomedicals, Eschwege, Germany). DMF was distilled and purged with argon prior to use. Other solvents were of reagent grade and were used without prior purification. Thymine, 3-chloropropionyl chloride, sodium hydride, methyl iodide, ytterbium(III) trifluoromethanesulfonate, potassium osmate(VI) dehydrate, hydroquinine 2,5-diphenyl-4,6-pyrimidinediyl diether [$(DHQ)_2Pyr$], hydroquinidine-2,5-diphenyl-4,6-pyrimidinediyl diether [$(DHQD)_2Pyr$], and potassium hexacyanoferrate(III) were purchased from commercial suppliers and were used without further purification. ^{1}H NMR (600 MHz) and ^{13}C{H} NMR (150 MHz) spectra were recorded with a Bruker Avance III 600 spectrometer operating at 298 K in the Fourier transform mode. Chemical shifts δ are reported in ppm using residual DMSO as reference (^{1}H $\delta=2.50$ ppm, ^{13}C $\delta=39.70$ ppm). Mass spectra were recorded using electron impact MS methods on a Finnigan MAT 95 mass spectrometer. IR spectra were recorded on a FTIR Nexus Nicolet instrument. Microanalyses were performed by the Analytical Services of the Polish Academy of the Sciences (Łódź). HPLC analyses were performed with a Shimadzu Prominence system equipped with photodiode array detector and using a Phenomenex Lux Cellulose-3 column 4.6×150 mm [for samples of (*S*,*R*)-**1** and (*R*,*S*)-**1**] or Lux Amylose-2 column 4.6×150 mm [for samples of (*S*,*R*)-**2** and (*R*,*S*)-**2**]. Detection was accomplished at $\lambda=254$ nm and a flow rate of 0.2 mL min^{-1} was applied. The ^{1}H and ^{13}C NMR spectra of studied compounds are shown in Figures S1–S4 and S5–S8, respectively.

UV/Vis absorption and circular dichroism spectroscopy

UV/Vis absorption spectra were recorded in a 10 mm quartz cell (Suprasil high-precision cell, Hellma GmbH, Müllheim, Germany) within the 250–800 nm wavelength region using a Thermo Scientific Evolution 220 UV/Vis spectrophotometer. Circular dichroism spectra were recorded in the wavelength range of 250–800 nm on a Jasco J-815-150S spectropolarimeter, with 2 nm steps and a dwell time of 2 s per step, using the same 10 mm quartz cell as described above. The complexes were dissolved in dichloromethane ($\approx5\times10^{-3}$ mol L^{-1}). The measured spectra were baseline-corrected with the solvent spectrum. Camphorsulfonic acid served as a calibration material for the CD instrument.

DFT calculations

All geometries were optimized at the B3LYP level of theory, as implemented in the Gaussian 09 software package.[52] The basis set for optimization was standard Pople's 6-31G(d) on nonmetal atom centers, whereas the Stuttgart–Dresden (SDD)[53] basis set with effective core potential was used for Fe, similar to previous studies.[54] Harmonic frequencies were computed from analytical second derivatives at the corresponding level of theory.

Implicit solvation effects were determined using the SMD continuum solvation model at the same B3LYP level, with the UFF atomic radii and electrostatic scaling factor (alpha value) set to 1.1 for all atoms (default values in Gaussian 09).[55,56] The solvent relative permittivity of $\varepsilon=8.93$ (dichloromethane) was used. Formal redox potentials were calculated at the B3LYP/6-31G(d)/SDD level of theory, using the protocol scheme deposited in the Supporting Information.

TD-DFT calculations were performed using Becke's exchange functional[57] and the Perdew–Wang correlation functional (BPW91).[58] The basis set for the excitation energies calculation was the standard Pople's 6-311G(d) on nonmetal atom centers, whereas the SDD basis set was used for Fe. The lowest 20 singlet excited energies were calculated.

Electrochemistry

Electrochemical measurements on dichloromethane solutions of (*S*,*R*)-**1**, (*R*,*S*)-**1**, (*S*,*R*)-**2**, and (*R*,*S*)-**2** (1.0 mmol L^{-1}) were performed at 25 °C with a Radiometer Voltalab PGZ 100 electrochemical worksta-

tion interfaced with a personal computer. Dimethyl sulfoxide (0.1 mol L^{-1}) containing $[NBu_4][B(C_6F_5)_4]$[59] was used as supporting electrolyte. For the measurements a three-electrode cell was used containing a Pt auxiliary electrode, a glassy carbon working electrode (surface area 0.031 cm^2) and a Ag/Ag^+ ($AgNO_3$, 0.01 mmol L^{-1}) reference electrode fixed on a Luggin capillary. The working electrode was pretreated by polishing on a Buehler microcloth first with a 1 μm and then a 0.25 μm diamond paste. The reference electrode was constructed as previously described.[60] Experiments under the same conditions showed that all reduction and oxidation potentials were reproducible within 5 mV. Experimental potentials were referenced against a Ag/Ag^+ reference electrode, but the presented results are referenced against ferrocene as an internal standard, as required by IUPAC.[51] To achieve this, each experiment was repeated in the presence of decamethylferrocene (Fc*, 1 mmol L^{-1}). Data were processed on a Microsoft Excel worksheet to set the formal reduction potentials of the FcH/FcH^+ couple to 0.0 V. Under our conditions, the Fc^*/Fc^{*+} couple was at −469 mV versus FcH/FcH^+ ($\Delta E_p = 60$ mV).

Synthesis of thymine olefin B

Ytterbium(III) trifluoromethanesulfonate (19 mg, 0.03 mmol) was added in a single portion to a stirred solution of thymine alcohol **A** (110 mg, 0.30 mmol) in ethylene glycol (60 mL) at ambient temperature. The resulting reaction mixture was stirred at 110 °C for 20 h. After cooling to ambient temperature, the reaction was quenched with water (10 mL) and the obtained mixture was extracted with chloroform. The organic layer was separated in a separating funnel, dried over anhydrous $MgSO_4$, filtered through a Schott funnel and then all volatile materials were evaporated. The residue was subjected to column chromatography on SiO_2 (dichloromethane/methanol, 50:1 v/v). Crystallization from dichloromethane/*n*-hexane gave the pure **B** as orange-yellow crystals (69 mg, 66% yield). For spectral data, see Ref. [37].

General procedure for the synthesis of nucleosides (*S*,*R*)-1 and (*R*,*S*)-1

The thymine olefin **B** (105 mg, 0.30 mmol), $(DHQ)_2Pyr$ or $(DHQD)_2Pyr$ (26 mg, 0.03 mmol), potassium osmate(VI) dehydrate (4 mg, 0.01 mmol), potassium hexacyanoferrate(III) (296 mg, 0.90 mmol), K_2CO_3 (124 mg, 0.90 mmol) and a water/acetonitrile (1:1 v/v) mixture was placed in a Schlenk flask. The reaction mixture was stirred at ambient temperature for 3 h. Then, $Na_2SO_3 \cdot 7H_2O$ (681 mg, 2.70 mmol) was added in a single portion and the reaction mixture was stirred for 20 min, Then it was extracted with chloroform. The organic layer was separated in a separating funnel, dried over anhydrous $MgSO_4$, filtered through a Schott funnel and then all volatile materials were evaporated under reduced pressure. The residue was subjected to column chromatography on SiO_2 (dichloromethane/methanol, 50:1 v/v). Chromatographically purified nucleosides (*S*,*R*)-**1** and (*R*,*S*)-**1** were crystallized from a mixture of dichloromethane/methanol/*n*-heptane to afford analytically pure samples. Isomer (*S*,*R*)-**1** was obtained as a yellow crystalline solid (83 mg, 72% yield); *ee* > 99% by HPLC ($\tau = 20.27$ min). Isomer (*R*,*S*)-**1** was obtained as a yellow crystalline solid (80 mg, 70% yield); *ee* = 71% by HPLC ($\tau = 19.44$ min).

1: ^1H NMR (600 MHz, [D_6]DMSO): $\delta = 11.14$ (s, 1H; NH), 7.33(s, 1H; thymine), 4.81(d, $J_{H,H} = 6.0$ Hz, 1H; OH), 4.79 (d, $J_{H,H} = 6.6$ Hz, 1H; OH), 4.29 (brs, 2H; C_5H_4), 4.26 (brs, 1H; CH), 4.15 (s, 5H; C_5H_5), 4.08 (brs, 2H; C_5H_4), 3.88–3.82 (m, 2H; CH and 1H CH_2), 3.30 (s; H_2O overlapped with 1H CH_2), 1.73 ppm (s, 3H; thymine CH_3); $^{13}C\{^1H\}$ NMR (150 MHz, [D_6]DMSO): $\delta = 164.5$, 151.2, 143.0, 107.4, 90.0, 71.5, 70.2, 68.5, 67.4, 67.3, 67.2, 67.0, 51.3, 12.0 ppm; FTIR (KBr): $\tilde{\nu} = 3351$, 3167, 3056, 2955, 2920, 1698, 1673, 1474, 1369 cm^{-1}; MS (EI): *m*/*z*: 384 $[M]^+$, 366 $[M-H_2O]^+$; elemental analysis calcd (%) for $C_{18}H_{20}N_2O_4Fe$: C 56.27, H 5.25, N 7.29; found: (*S*,*R*)-**1**: C 56.39, H 5.51, N 7.24; (*R*,*S*)-**1**: C 56.31, H 5.19, N 7.26.

General procedure for the synthesis of methylated nucleosides (*S*,*R*)-2 and (*R*,*S*)-2

Sodium hydride (22 mg, 0.90 mmol) was added in a single portion to a stirred solution of either (*S*,*R*)-**1** or (*R*,*S*)-**1** (115 mg, 0.30 mmol) in anhydrous DMF (30 mL). After stirring the reaction mixture for 2 h, CH_3I (128 mg, 0.90 mmol, 56 μL) was added in a single portion and the reaction mixture was stirred at ambient temperature for 20 h. Subsequently, water (≈10 mL) was added and the reaction mixture was extracted with chloroform. The organic layer was separated in a separating funnel, dried over anhydrous $MgSO_4$, filtered through a Schott funnel and all volatiles were evaporated under reduced pressure. The remaining solid was subjected to column chromatography on deactivated Al_2O_3 (Al_2O_3/H_2O, 30/1.25 g) with diethyl ether as eluent. Crystallization from a dichloromethane/*n*-pentane mixture gave analytically pure samples. Isomer (*S*,*R*)-**2** was obtained as a yellow crystalline solid (42 mg, 33% yield); *ee* > 99% by HPLC ($\tau = 12.68$ min). Isomer (*R*,*S*)-**2** was obtained as a yellow crystalline solid (43 mg, 34% yield); *ee* 90% by HPLC ($\tau = 12.27$ min).

2: ^1H NMR (600 MHz, [D_6]DMSO): $\delta = 7.36$ (s, 1H; thymine), 4.25 (brs, 1H; C_5H_4), 4.21 (brs, 1H; C_5H_4), 4.17 (s, 7H; C_5H_5 and C_5H_4), 4.16 (d, $J_{H,H} = 3.6$ Hz, 1H; Fc-C<u>H</u>OMe), 3.92 (dd, $J_{H,H} = 13.8$, 3.6 Hz, 1H; CH_2), 3.76 (dt, $J_{H,H} = 8.4$, 3.6 Hz, 1H; Fc-CH(OMe)C<u>H</u>OMe), 3.46 (s, 3H; CH_3), 3.34 (dd, $J_{H,H} = 13.8$, 8.4 Hz, 1H; CH_2), 3.27 (s, 3H; CH_3), 3.18 (s, 3H; CH_3), 1.79 ppm (s, 3H; CH_3); $^{13}C\{^1H\}$ NMR (150 MHz, [D_6]DMSO): $\delta = 163.5$, 151.2, 140.9, 107.0, 85.7, 80.2, 78.0, 68.7, 67.8, 67.4, 67.1, 67.0, 58.4, 57.8, 49.9, 27.6, 12.6 ppm; FTIR (KBr): $\tilde{\nu} =$ 3090, 2978, 2933, 2827, 1698, 1666, 1640, 1468, 1368 cm^{-1}; EI-MS (EI): *m*/*z*: 426 $[M]^+$; elemental analysis calcd (%) for $C_{21}H_{26}N_2O_4Fe$: C 59.17, H 6.15, N 6.57; found: (*S*,*R*)-**2**: C 59.20, H 6.31, N 6.42; (*R*,*S*)-**2**: C 59.42, H 6.31, N 6.20.

X-ray data collection and refinement of data

Good-quality single crystals of (*S*,*R*)-**2** and (*R*,*S*)-**2** were selected for the X-ray diffraction experiments at $T = 100(2)$ K. Diffraction data were collected on the Agilent Technologies SuperNova Dual Source diffractometer with CuKα radiation ($\lambda = 1.54184$ Å) using CrysAlis RED software.[61] In all cases the analytical numerical absorption correction using a multifaceted crystal model based on expressions derived by Clark and Reid[62] and implemented in the SCALE3 ABSPACK scaling algorithm was applied.[61] The structural determination procedure was carried out using the SHELX package.[63] The structures were solved with direct methods and then successive least-square refinement was carried out based on the full-matrix least-squares method on F^2 using the XLMP program.[63] All H atoms were positioned geometrically, with C–H equal to 0.93, 0.96, 0.97 and 0.98 Å for the aromatic, methyl, methylene and methine H atoms, respectively, and constrained to ride on their parent atoms with $U_{iso}(H) = xU_{eq}(C)$, where $x = 1.2$ for the aromatic, methylene and methine H atoms, and $x = 1.5$ for the methyl H atoms. The figures for this publication were prepared using Olex2, Mercury

and ORTEP-3 programs.[64–66] The molecular interactions were identified using PLATON.[67]

CCDC 1585503 and 1585502 contain the supplementary crystallographic data for this paper. These data are provided free of charge by The Cambridge Crystallographic Data Centre.

Acknowledgements

The X-ray single-crystal diffraction analysis was carried out at the Biological and Chemical Research Centre, University of Warsaw, established within the project co-financed by the European Union from the European Regional Development Fund under the Operational Programme Innovative Economy, 2007–2013. This research was supported by NCN (Polish National Center of Science) grants 2013/09/B/NZ3/01389,2012/05/E/ST2/02180 (TB) and MAESTRO grant-DEC-2012/04/A/ST5/00609 (D.T. and K.W. for structural analysis). V.V. thanks the Croatian Science Foundation for financial support (project no. IP-2016-06-1137).

Conflict of interest

The authors declare no conflict of interest.

Keywords: bioorganometallic compounds · ferrocene · glycol nucleic acids · nucleosides · xeno-nucleic acids

[1] O. Doluca, J. M. Withers, V. V. Filichev, *Chem. Rev.* **2013**, *113*, 3044 – 3083.
[2] O. I. Wilner, I. Willner, *Chem. Rev.* **2012**, *112*, 2528 – 2556.
[3] T. Carell, C. Brandmayr, A. Hienzsch, M. Müller, D. Pearson, V. Reiter, I. Thoma, P. Thumbs, M. Wagner, *Angew. Chem. Int. Ed.* **2012**, *51*, 7110 – 7131; *Angew. Chem.* **2012**, *124*, 7220 – 7242.
[4] B. Roy, A. Depaix, C. Périgaud, S. Peyrottes, *Chem. Rev.* **2016**, *116*, 7854 – 7897.
[5] P. Perlíková, M. Hocek, *Med. Res. Rev.* **2017**, *37*, 1429 – 1460.
[6] J. Shelton, X. Lu, J. A. Hollenbaugh, J. H. Cho, F. Amblard, R. Schinazi, *Chem. Rev.* **2016**, *116*, 14379 – 14455.
[7] P. Herdewijn, P. Marlière, *Chem. Biodiversity* **2009**, *6*, 791 – 808.
[8] V. B. Pinheiro, P. Hollinger, *Curr. Opin. Chem. Biol.* **2012**, *16*, 245 – 252.
[9] V. B. Pinheiro, A. I. Taylor, C. Cozens, M. Abramov, M. Renders, S. Zhang, J. C. Chaput, J. Wengel, S.-Y. Peak-Chew, S. H. McLaughlin, P. Herdewijn, P. Hollinger, *Science* **2012**, *336*, 341 – 344.
[10] L. Zhang, A. Peritz, E. Meggers, *J. Am. Chem. Soc.* **2005**, *127*, 4174 – 4175.
[11] M. K. Schlegel, A. E. Peritz, K. Kittigowittana, L. Zhang, E. Meggers, *ChemBioChem* **2007**, *8*, 927 – 932.
[12] M. K. Schlegel, L.-O. Essen, E. Meggers, *J. Am. Chem. Soc.* **2008**, *130*, 8158 – 8159.
[13] E. Meggers, L. Zhang, *Acc. Chem. Res.* **2010**, *43*, 1092 – 1102.
[14] G. F. Joyce, A. W. Schwartz, S. L. Miller, L. E. Orgel, *Proc. Natl. Acad. Sci. USA* **1987**, *84*, 4398 – 4402.
[15] B. D. Heuberger, C. Switzer, *J. Am. Chem. Soc.* **2008**, *130*, 412 – 413.
[16] A. M. Noronha, C. J. Wilds, C.-N. Lok, K. Viazovkina, D. Arion, M. A. Parniak, M. J. Damha, *Biochemistry* **2000**, *39*, 7050 – 7062.
[17] C. J. Wilds, M. J. Damha, *Nucleic Acids Res.* **2000**, *28*, 3625 – 3635.
[18] K.-U. Schöning, P. Scholz, S. Guntha, X. Wu, R. Krishnamurthy, A. Eschenmoser, *Science* **2000**, *290*, 1347 – 1351.
[19] D. Zhou, I. M. Lagoja, J. Rozenski, R. Busson, A. Van Aerschot, P. Herdewijn, *ChemBioChem* **2005**, *6*, 2298 – 2304.
[20] H. Asanuma, T. Toda, K. Murayama, X. Liang, H. Kashida, *J. Am. Chem. Soc.* **2010**, *132*, 14702 – 14703.
[21] K. Toti, M. Renders, E. Groaz, P. Herdewijn, S. Van Calenbergh, *Chem. Rev.* **2015**, *115*, 13484 – 13525.
[22] M. A. Campbell, J. Wengel, *Chem. Soc. Rev.* **2011**, *40*, 5680 – 5689.
[23] M. Egli, P. S. Pallan, R. Pattanayek, C. J. Wilds, P. Lubini, G. Minasov, M. Dobler, C. J. Leumann, A. Eschenmoser, *J. Am. Chem. Soc.* **2006**, *128*, 10847 – 10856.
[24] R. Declercq, A. Van Aerschot, R. J. Read, P. Herdewijn, L. Van Meervelt, *J. Am. Chem. Soc.* **2002**, *124*, 928 – 933.
[25] J. Wang, B. Verbeure, I. Luyten, E. Lescrinier, M. Froeyen, C. Hendrix, H. Rosemeyer, F. Seela, A. Van Aerschot, P. Herdewijn, *J. Am. Chem. Soc.* **2000**, *122*, 8595 – 8602.
[26] S. Paul, M. H. Caruthers, *J. Am. Chem. Soc.* **2016**, *138*, 15663 – 15672.
[27] a) *Chiral Ferrocenes in Asymmetric Catalysis* (Eds.: L.-X. Dai, X.-L. Hou), Wiley-VCH, Weinheim, **2010**; b) D. Schaarschmidt, M. Grumbt, A. Hildebrandt, H. Lang, *Eur. J. Inorg. Chem.* **2014**, 6676 – 6685; c) C. Gäbler, J. M. Speck, M. Korb, D. Schaarschmidt, H. Lang, *J. Organomet. Chem.* **2016**, *813*, 26 – 35.
[28] a) I. Manners, *Synthetic Metal-Containing Polymers*, Wiley-VCH, Weinheim, **2004**; b) J. M. Speck, D. Schaarschmidt, H. Lang, *Organometallics* **2012**, *31*, 1975 – 1982; c) M. Lohan, F. Justaud, H. Lang, C. Lapinte, *Organometallics* **2012**, *31*, 3565 – 3574; d) K. Kowalski, R. Karpowicz, G. Mlostoń, D. Miesel, A. Hildebrandt, H. Lang, R. Czerwieniec, B. Therrien, *Dalton Trans.* **2015**, *44*, 6268 – 6276; e) M. S. Inkpen, S. Scheerer, M. Linseis, A. J. P. White, R. F. Winter, T. Albrecht, N. J. Long, *Nat. Chem.* **2016**, *8*, 825 – 830.
[29] a) N. Metzler-Nolte, M. Salmain in *Ferrocenes: Ligands, Materials and Biomolecules* (Ed.: P. Štěpnička), John Wiley & Sons Ltd., Chichester, **2008**, pp. 499 – 639; b) K. Heinze, H. Lang, *Organometallics* **2013**, *32*, 5623 – 6146; c) P. Štepnička, *Eur. J. Inorg. Chem.* **2017**, 212 – 526.
[30] a) G. Jaouen, A. Vessières, S. Top, *Chem. Soc. Rev.* **2015**, *44*, 8802 – 8817; b) Y. Wang, P. Pigeon, S. Top, M. J. McGlinchey, G. Jaouen, *Angew. Chem. Int. Ed.* **2015**, *54*, 10230 – 10233; *Angew. Chem.* **2015**, *127*, 10368 – 10371; c) P. Pigeon, Y. Wang, S. Top, F. Najlaoui, M. C. G. Alvarez, J. Bignon, M. J. McGlinchey, G. Jaouen, *J. Med. Chem.* **2017**, *60*, 8358 – 8368.
[31] a) F. Dubar, C. Biot in *Bioorganometallic Chemistry, Applications in Drug Discovery, Biocatalysis, and Imaging* (Eds.: G. Jaouen, M. Salmain), Wiley-VCH, Weinheim, **2015**, Chapter 5, pp. 141 – 164; b) N. Metzler-Nolte in *Bioorganometallics: Biomolecules, Labeling, Medicine* (Ed.: G. Jaouen), Wiley-VCH, Weinheim, **2006**, Chapter 5, pp. 125 – 179; c) M. Patra, G. Gasser, *Nat. Rev. Chem.* **2017**, *1*, 0066; d) B. Albada, N. Metzler-Nolte, *Chem. Rev.* **2016**, *116*, 11797 – 11839; e) G. Gasser, I. Ott, N. Metzler-Nolte, *J. Med. Chem.* **2011**, *54*, 3 – 25.
[32] J. L. Kedge, H. V. Nguyen, Z. Khan, L. Male, M. K. Ismail, H. V. Roberts, N. J. Hodges, S. L. Horswell, Y. Mehellou, J. H. R. Tucker, *Eur. J. Inorg. Chem.* **2017**, 466 – 476.
[33] H. V. Nguyen, A. Sallustrau, J. Balzarini, M. R. Bedford, J. C. Eden, N. Georgousi, N. J. Hodges, J. Kedge, Y. Mehellou, C. Tselepis, J. H. R. Tucker, *J. Med. Chem.* **2014**, *57*, 5817 – 5822.
[34] J.-L. H. A. Duprey, J. H. R. Tucker, *Chem. Lett.* **2014**, *43*, 157 – 163.
[35] H. V. Nguyen, Z. Zhao, A. Sallustrau, S. L. Horswell, L. Male, A. Mulas, J. H. R. Tucker, *Chem. Commun.* **2012**, *48*, 12165 – 12167.
[36] I. Anisimov, S. Saloman, A. Hildebrandt, H. Lang, D. Trzybiński, K. Woźniak, D. Šakić, V. Vrček, K. Kowalski, *ChemPlusChem* **2017**, *82*, 859 – 866.
[37] K. Kowalski, J. Skiba, L. Oehninger, I. Ott, J. Solecka, A. Rajnisz, B. Therrien, *Organometallics* **2013**, *32*, 5766 – 5773.
[38] H. C. Kolb, M. S. Van Nieuwenhze, K. B. Sharpless, *Chem. Rev.* **1994**, *94*, 2483 – 2547.
[39] W. G. Jary, J. Baumgartner, *Tetrahedron: Asymmetry* **1998**, *9*, 2081 – 2085.
[40] K. Kowalski, Ł. Szczupak, J. Skiba, O. S. Abdel-Rahman, R. F. Winter, R. Czerwieniec, B. Therrien, *Organometallics* **2014**, *33*, 4697 – 4705.
[41] K. Kowalski, M. Linseis, R. F. Winter, M. Zabel, S. Záliš, H. Kelm, H.-J. Krüger, B. Sarkar, W. Kaim, *Organometallics* **2009**, *28*, 4196 – 4209.
[42] J. Tauchman, K. Hladíková, F. Uhlík, I. Císarová, P. Štěpnička, *New J. Chem.* **2013**, *37*, 2019 – 2030.
[43] K. Kowalski, R. F. Winter, *J. Organomet. Chem.* **2009**, *694*, 1041 – 1048.
[44] J. C. Calabrese, L.-T. Cheng, J. C. Green, S. R. Marder, W. Tam, *J. Am. Chem. Soc.* **1991**, *113*, 7227 – 7232.
[45] V. N. Nemykin, A. Y. Maximov, A. Y. Koposov, *Organometallics* **2007**, *26*, 3138 – 3148.
[46] M. Kovačević, I. Kodrin, M. Cetina, I. Kmetič, T. Murati, M. Č. Semenčić, S. Roca, L. Barišić, *Dalton Trans.* **2015**, *44*, 16405 – 16420.
[47] S. Brahma, S. A. Ikbal, A. Dhamija, S. P. Rath, *Inorg. Chem.* **2014**, *53*, 2381 – 2395.

[48] S. I. Kirin, D. Wissenbach, N. Metzler-Nolte, *New J. Chem.* **2005**, *29*, 1168 – 1173.
[49] M. Iurlo, L. Mengozzi, S. Rapino, M. Marcaccio, R. C. Perone, S. Masiero, P. Cozzi, F. Paolucci, *Organometallics* **2014**, *33*, 4986 – 4993.
[50] J. Kondo, Y. Tada, T. Dairaku, Y. Hattori, H. Saneyoshi, A. Ono, Y. Tanaka, *Nat. Chem.* **2017**, *9*, 956 – 960.
[51] G. Gritzner, J. Kuta, *Pure Appl. Chem.* **1984**, *56*, 461 – 466.
[52] Gaussian 09, Revision D.01, M. J. Frisch, G. W. Trucks, H. B. Schlegel, G. E. Scuseria, M. A. Robb, J. R. Cheeseman, G. Scalmani, V. Barone, B. Mennucci, G. A. Petersson, H. Nakatsuji, M. Caricato, X. Li, H. P. Hratchian, A. F. Izmaylov, J. Bloino, G. Zheng, J. L. Sonnenberg, M. Hada, M. Ehara, K. Toyota, R. Fukuda, J. Hasegawa, M. Ishida, T. Nakajima, Y. Honda, O. Kitao, H. Nakai, T. Vreven, J. A. Montgomery, Jr., J. E. Peralta, F. Ogliaro, M. Bearpark, J. J. Heyd, E. Brothers, K. N. Kudin, V. N. Staroverov, R. Kobayashi, J. Normand, K. Raghavachari, A. Rendell, J. C. Burant, S. S. Iyengar, J. Tomasi, M. Cossi, N. Rega, J. M. Millam, M. Klene, J. E. Knox, J. B. Cross, V. Bakken, C. Adamo, J. Jaramillo, R. Gomperts, R. E. Stratmann, O. Yazyev, A. J. Austin, R. Cammi, C. Pomelli, J. W. Ochterski, R. L. Martin, K. Morokuma, V. G. Zakrzewski, G. A. Voth, P. Salvador, J. J. Dannenberg, S. Dapprich, A. D. Daniels, Ö. Farkas, J. B. Foresman, J. V. Ortiz, J. Cioslowski, D. J. Fox, Gaussian, Inc., Wallingford, CT, **2009**.
[53] M. Dolg, U. Wedig, H. Stoll, H. Preuß, *J. Chem. Phys.* **1987**, *86*, 866 – 872.
[54] T. Romero, A. Caballero, A. Espinosa, A. Tárraga, P. Molina, *Dalton Trans.* **2009**, 2121 – 2129.
[55] M. Cossi, G. Scalmani, N. Rega, V. Barone, *J. Chem. Phys.* **2002**, *117*, 43 – 54.
[56] V. Barone, M. Cossi, J. Tomasi, *J. Chem. Phys.* **1997**, *107*, 3210 – 3221.
[57] A. D. Becke, *Phys. Rev. A* **1988**, *38*, 3098 – 3100.
[58] J. P. Perdew, K. Burke, Y. Wang, *Phys. Rev. B* **1996**, *54*, 16533 – 16539.
[59] a) D. Miesel, A. Hildebrandt, M. Korb, D. Schaarschmidt, H. Lang, *Organometallics* **2015**, *34*, 4293 – 4304; b) M. I. R. Valderrama, R. A. V. García, T. Klimova, E. Klimova, L. Ortiz-Frade, M. M. García, *Inorg. Chim. Acta* **2008**, *361*, 1597 – 1605; c) R. J. LeSuer, C. Buttolph, W. E. Geiger, *Anal. Chem.* **2004**, *76*, 6395 – 6401; d) F. Barrière, W. E. Geiger, *J. Am. Chem. Soc.* **2006**, *128*, 3980 – 3989; e) J. C. Swarts, A. Nafady, J. H. Roudebush, S. Trupia, W. E. Geiger, *Inorg. Chem.* **2009**, *48*, 2156 – 2165; f) V. N. Nemykin, G. T. Rohde, C. D. Barrett, R. G. Hadt, J. R. Sabin, G. Reina, P. Galloni, B. Floris, *Inorg. Chem.* **2010**, *49*, 7497 – 7509.
[60] a) A. Hildebrandt, D. Schaarschmidt, H. Lang, *Organometallics* **2011**, *30*, 556 – 563; b) A. Hildebrandt, K. Al Khalyfeh, D. Schaarschmidt, M. Korb, *J. Organomet. Chem.* **2016**, *804*, 87 – 94; c) U. Pfaff, G. Filipczyk, A. Hildebrandt, M. Korb, H. Lang, *Dalton Trans.* **2014**, *43*, 16310 – 16321.
[61] CrysAlis CCD and CrysAlis RED, Oxford Diffraction, Oxford Diffraction Ltd, Yarnton, UK, **2008**.
[62] R. C. Clark, J. S. Reid, *Acta Crystallogr. Sect. A* **1995**, *51*, 887 – 897.
[63] G. M. Sheldrick, *Acta Crystallogr. Sect. A* **2008**, *64*, 112 – 122.
[64] O. V. Dolomanov, L. J. Bourhis, R. J. Gildea, J. A. K. Howard, H. Puschmann, *J. Appl. Crystallogr.* **2009**, *42*, 339 – 341.
[65] C. F. Macrae, I. J. Bruno, J. A. Chisholm, P. R. Edgington, P. McCabe, E. Pidcock, L. Rodriguez-Monge, R. Taylor, J. van de Streek, P. A. Wood, *J. Appl. Crystallogr.* **2008**, *41*, 466 – 470.
[66] L. J. Farrugia, *J. Appl. Crystallogr.* **2012**, *45*, 849 – 854.
[67] A. L. Spek, *Acta Crystallogr. Sect. D* **2009**, *65*, 148 – 155.

Manuscript received: December 20, 2017
Revised manuscript received: January 19, 2018
Accepted manuscript online: January 23, 2018